# Focussed helium ion channeling through Si nanomembranes

Jiaming Wang, Symphony H. Y. Huang, Christoph Herrmann, Shelley A. Scott, François Schiettekatte, and Karen L. Kavanagh

Citation: Journal of Vacuum Science & Technology B, Nanotechnology and Microelectronics: Materials, Processing, Measurement, and Phenomena **36**, 021203 (2018); doi: 10.1116/1.5020667

View online: https://doi.org/10.1116/1.5020667

View Table of Contents: http://avs.scitation.org/toc/jvb/36/2

Published by the American Vacuum Society

# Focussed helium ion channeling through Si nanomembranes


Jiaming Wang, Symphony H. Y. Huang, and Christoph Herrmann
*Department of Physics, Simon Fraser University, Burnaby, British Columbia V5A 1S6, Canada*

Shelley A. Scott
*Department of Materials Science and Engineering, University of Wisconsin-Madison, Madison, Wisconsin 53706*

François Schiettekatte
*Department of Physics, University of Montreal, Montreal, Quebec, Canada H3T 1J4*

Karen L. Kavanagh[a)]
*Department of Physics, Simon Fraser University, Burnaby, British Columbia V5A 1S6, Canada*



(Received 25 December 2017; accepted 1 March 2018; published 14 March 2018)



Channeling of low energy (25 to 35 keV) focussed He ions transmitted through crystalline Si (001) nanomembranes (50 nm) has been observed using a He ion microscope. Planar (110) and (100) channeling was detected with critical incident angles of 1.0° at 35 keV. Beam steering of up to 2° occurs. The technique has potential for He ion diffraction and femtometer-scale detection of interstitial atoms and impurities. *Published by the AVS.* https://doi.org/10.1116/1.5020667


## I. INTRODUCTION

Focussed $He^+$ ions (5–40 keV) in the He ion microscope (HIM) generate low energy (50 eV) secondary electrons (SE) that originate within a few nanometers of the surface. Their intensity as a function of focussed beam position gives the common type of image obtained with this microscope with resolution <1 nm.[1]

For crystalline samples, the orientation of each grain can be mapped through the influence of channeling on the surface SE intensity.[2] Channeling is the reduction in scattering that occurs when a particle beam is directed along atomic rows in a crystal.[3,4] Alignment of an ion beam to be within a critical angle of a plane or row of atoms leads to fewer backscattering events, smaller energy loss, and deeper penetration into the crystal. The atomic rows act as a potential trap steering and maintaining the beam ions along these directions. Since the beam interacts with fewer surface atoms, the generation of SE by a channeled beam can be correlated with the orientation.

Annular dark-field scanning transmission ion microscopy has been demonstrated in a HIM via the addition of an annular, microchannel plate underneath the sample.[5] Like scanning transmission electron microscopy (TEM), this approach measures the intensity of transmitted particles after scattering a range of angles, dependent on the distance to the annular detector. Images with nanometer resolution are obtained, dependent on the beam spot size and sample interaction volume.

In this work, a digital camera was used in a HIM to collect transmission He ion microscopy images from stationary, $He^+$ ion beams forward scattered through Si nanomembranes, as a function of sample orientation and beam energy (25–35 keV). The digital camera measured the intensity as a function of both scattering angle and direction. Planar channeling and beam steering were observed and critical half-angles measured. Results were compared to simulations from theoretical modeling.

## II. EXPERIMENT AND SIMULATION

The HIM at Simon Fraser U (SFU) (Zeiss Orion Nanofab) was modified to conduct transmission experiments by adding a digital camera 20 cm below the stage at the bottom of the chamber.[6] The camera consists of a square array ($256 \times 256$ pixels) of uncooled, Si p-i-n diodes each $55 \times 55\ \mu m^2$ large. There is a common, n-type Si surface (no optical filter layer) exposed to the ion beam, while the p-type side of each diode is bump bonded to the amplifier circuitry below. Each diode is reverse biased (100 V) and can detect individual He ions with energies as low as 15 keV.

In a HIM, $He^+$ ions are accelerated after field emission via electrostatic lenses, which focus the beam (parallel to the $z$-direction) to a spot size less than 1 nm. Electrostatic deflectors scan or stop the beam at a particular location. The sample is mounted on a stage that moves $(x, y) = (\pm 25, \pm 25)$ mm and rotates 360° about an axis through its center. The stage sits on a larger "cradle" that tilts about the $x$-axis (+50 to –5)°. By cutting a slit in the side of the cradle, tilting it by $40 \pm 5°$, and moving the stage to one of its $(x, y)$ extension maxima, the beam can reach the camera without hitting any of this hardware. The samples are then held over the edge of the stage using a homemade extension arm which has a hole (3 mm diameter) and a $-45 \pm 5°$ fixed tilt. A schematic diagram of the modifications along the $x$-axis is shown in Fig. 1.

The samples for transmission measurements were $150\ \mu m^2$, free-standing, monocrystalline Si (001) nanomembranes[7,8] with their edges parallel to $\langle 110 \rangle$ directions. They were fabricated by thinning Si on insulator substrates, a procedure that can produce self-supporting nanomembranes as thin as 1.6 nm, over large areas ($>100\ \mu m^2$).[9] They can be relatively strain-free,[10] depending on the type of manufacture and care in handling.[7] Our membranes were mounted such that one edge was parallel to the $x$-axis, meaning that we could vary the beam orientation via sample tilt to align with a set of $\langle 110 \rangle$ planes. We did not remove the native oxide for these experiments. Measurements as a function of energy and beam tilt were performed on 50 nm thick membranes using a focussed $He^+$,


[a)]Electronic mail: kavanagh@sfu.ca

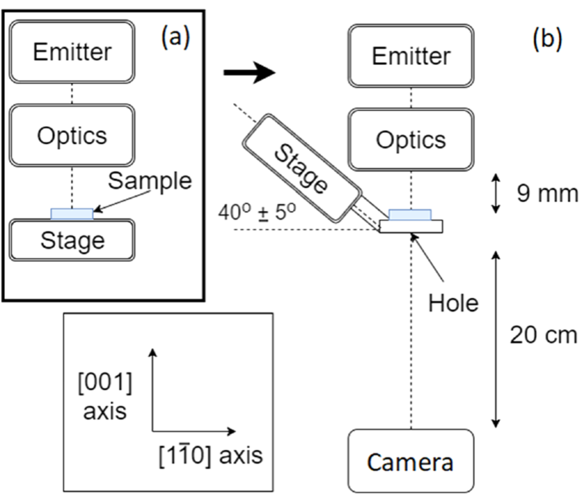


FIG. 1. (Color online) Diagrams showing the experimental set-up required to bypass the standard HIM stage (a) via a tilted extension arm (b). The arm has a hole (3 mm diameter) and a fixed tilt to counteract the opposite polarity tilt necessary to avoid hitting the cradle. The $x$-axis tilt in our experiments occurs through the sample perpendicular to the plane of the diagram.

0.35 pA beam. The spot size was less than 1 nm in diameter giving a fluence on the sample of $3 \times 10^{20}$ cm$^{-2}$ s$^{-1}$. At the camera, using a 20 $\mu$m condenser aperture, the He ion fluence decreases to $10^{8}$ cm$^{-2}$ s$^{-1}$ or $3 \times 10^{5}$ counts/pixel.[6] The integrated He counts on the camera were recorded for acceleration energies of 25, 27, 30, and 35 keV and tilt angles of between –7° and 3°. The beam was moved within the central region of the membrane for each tilt angle step to avoid development of beam-induced carbon formation.

Simulations of the experiment were carried out using large-scale atomic/molecular massively parallel simulator (LAMMPS),[11] considering a 50-nm-thick slab of (001) Si, a 30 keV He$^{+}$ ion beam, and using a mixed Ziegler-Biersack-Littmark (ZBL)-Tersoff potential proposed by Devanathan *et al.*[12] For He-Si interactions, only the ZBL potential was applied. Each simulation involved 10 000 incident ions uniformly spread between tilt angles of –8° to +2°. (More accurately, 20 batches of 500 ions were simulated at angular intervals of 0.02°, so there were 20 ions at each 0.02° interval.) The impact point of each of the 10 000 ions was selected randomly, and there was a different random seed for each simulation. It took 63 h on 20 processors featuring eight cores each, i.e., a bit less than 1 min/ion on an eight-core processor. Nine thousand seven hundred and fifty nine ions were transmitted (or 97.6%).

## III. RESULTS

Figure 2 shows focused scanning ion beam-induced, SE images of two Si (100) nanomembranes: (a) 50 nm (Norcada, Inc.) and (b) 25 nm (U. of Wisconsin-Madison) thick. The contrasting bands near the corners in (a) and flower patterns in (b) are due to strain exerted by the nanomembrane edges or contaminants introduced during their fabrication. Similar strain patterns were visible from the same nanomembranes observed using TEM (not shown). This variation in SE intensity shifted in position when the sample was tilted typical of the known effects of channeling on SE intensity.[2]

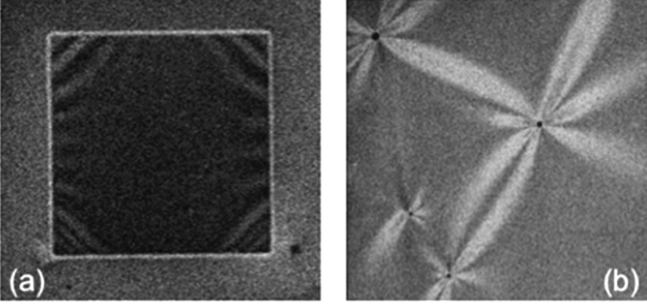


FIG. 2. Scanning focused He$^{+}$ ion beam induced, secondary electron images of Si (001) nanomembranes, (a) 50 nm and (b) 25 nm thick. The edge length is 150 $\mu$m in (a) and 100 $\mu$m in (b).

Figure 3 shows an example of a transmission He image through a 50 nm thick Si (001) membrane (Norcada), using the full camera area 256 × 256 pixels (1.41 × 1.41 mm$^{2}$). A static He$^{+}$ beam (0.35 pA) was focused on the Si nanomembrane in Fig. 2(a) near its center, and the camera collected counts during an exposure of 1 s. The image shows the intensity per pixel in a color scale as indicated by the contour lines. The beam center position, detected without the sample, is indicated by the cross near the top of the camera area. A two-dimensional profile along the $x$-direction is shown plotted in the inset. There is a broad transmitted peak centered in this case, 30 pixels from the unscattered position of the beam. Similar data were obtained as a function of the tilt angle and beam energy, all with beam currents of 0.35 pA. The maximum scattering angle, considering our geometry, was 4°.

It can be seen in the transmission image in Fig. 3 that the camera was purposely shifted off center to avoid aiming the beam at damaged pixel regions. There is a threshold beam

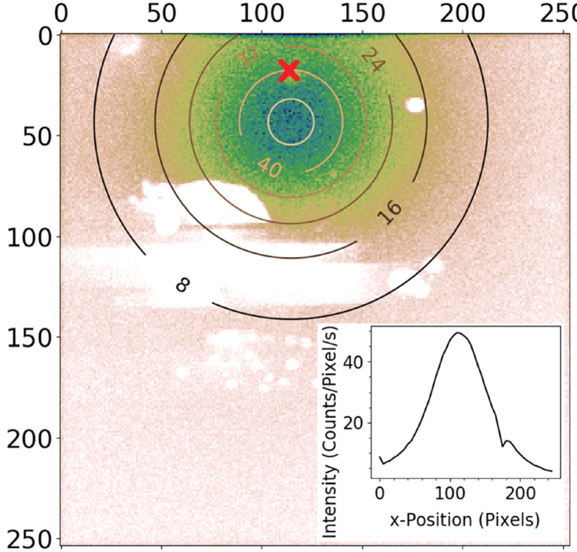


FIG. 3. (Color online) Transmission image through a Si (001) 50 nm thick membrane, for a 0.35 pA focussed He$^{+}$ beam (30 keV), showing counts/pixel/second across the Si camera (256 × 256 pixels square). The darkest pixels (blue online) represent the highest count range followed by a reduction in greyscale density to white. The contour lines show the fitted counts/pixel second, peaking at 45 counts/pixel s of the transmitted beam. The dead pixels (white areas) on the detector were omitted from the analysis. The beam position without the sample is indicated by the cross. The inset shows a line intensity profile along the x-direction through the peak region.

exposure that will damage individual camera pixels when exposed under bias. We subsequently have tried not to exceed 10 000 counts/pixel. The loss of sensitivity is likely related to He bubble formation and related defects known to degrade electrical conductivity.[13]

Each scattering map was fit to a normalized 2D Cauchy distribution. The center position, amplitude, integrated intensity, and full width at half maximum (FWHM) of the transmitted beam's intensity distribution were then extracted. The integrated intensity from the image in Fig. 3 (0.52 M counts/s) can be compared to the beam current (0.35 pA) equivalent to 2.2 M ions/s, a 24% fraction. We expect close to 100% transmission of 35 keV He through 50 nm of amorphous Si, with energy loss of 5 keV, according to calculations using stopping and range of ions in matter (SRIM) (Ref. 14) calculations. Some of our beam scattered outside the solid angle of the camera or into dead pixels and was not counted. The integrated 2D fit, assuming an infinite scattering area, gives a total scattered current of 0.8 M counts/s, or 60% of the beam current.

Most of the missed ions are likely explained by a decreasing camera efficiency with decreasing energy. By efficiency we mean the ratio of (count/s)*e* to beam current. Figure 4 shows a plot of measured camera efficiency (right y-axis) and average He ion range (left y-axis) from a SRIM calculation, as a function of beam energy, for 0.35 pA, 0.1 s exposures (no sample). The efficiency decreases from 100% at 35 keV to 55% at 25 keV. The linear decrease with decreasing beam energy is known to be partially due to an energy-independent, nuclear energy loss factor that reduces the rate of electron–hole pair formation.[15] Another likely factor in our case is the presence of a dead layer, in addition to the 2 nm thick native oxide layer. He ions with energies smaller than 15 keV are not detected, which is surprising, unless they are not penetrating past a surface dead layer. The average He ion range at 15 keV is only 100 nm in Si, so we suspect the presence of a 100 nm thick dead layer.

The fraction of the beam deflected by $>1^\circ$ as a function of tilt angle and beam energy was calculated from the FWHM and has been plotted in Fig. 5(a). Also plotted are similar data from an amorphous-Si nanomembrane (15 nm thick). Two dips in the plot are observed for the crystalline nanomembrane, spaced by $5.8 \pm 0.5^\circ$, while no variation is observed for the amorphous Si nanomembrane. We have assigned a tilt angle of zero to the center position of the largest dip in the plot which we will show is due to planar channeling along [110] planes in the sample. The depth of each dip increased with energy, and the FWHM of the right dip is smaller than that of the left.

The transmitted beam center, $x$ and $y$ positions, with respect to the incident beam position, versus the sample tilt angle are plotted in Figs. 6(a) and 6(b), respectively. In both cases, the left axis is in units of camera pixels while the right is converted into an angular value, based on the area of each pixel and their distance to the sample (20 cm). It is clear that the location of the beam center on the camera varied with the tilt angle. When the beam position is unchanged from the incident beam location, this is also where the largest

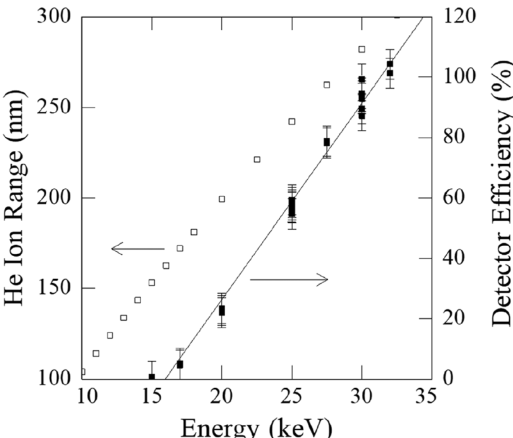


Fig. 4. Plot of the average He ion range (left axis) and camera efficiency (right axis) as a function of beam energy. The solid line overlaid is a least squared linear fit.

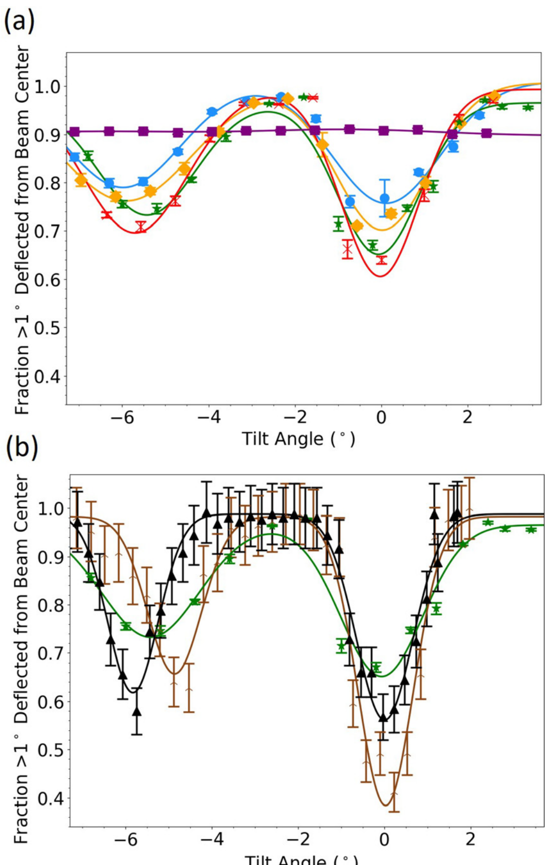


Fig. 5. (Color online) (a) Fraction deflected by greater than 1° as a function of sample tilt angle, and beam energy: 25 keV (circles, blue), 27 keV (diamonds, orange), 30 keV (stars, green), and 35 keV (x's, red), for transmission through a 50 nm Si (001) membrane, 0.35 pA current. Also shown for comparison is transmission of a 30 keV beam $He^+$ beam (squares, purple) through an amorphous Si nanomembrane (15 nm). The solid lines are double Gaussian fits to the data. (b) The data from 30 keV transmission through a Si membrane (stars, green) from (a) are replotted overlaid by two LAMMP simulations (beam energy of 30 keV) for horizontal tilt angles of 5° (upward arrow, brown) no oxide layers, and 5.8° (triangles, black) with 1 nm thick, amorphous Si oxide layers added on top and bottom of the membrane.

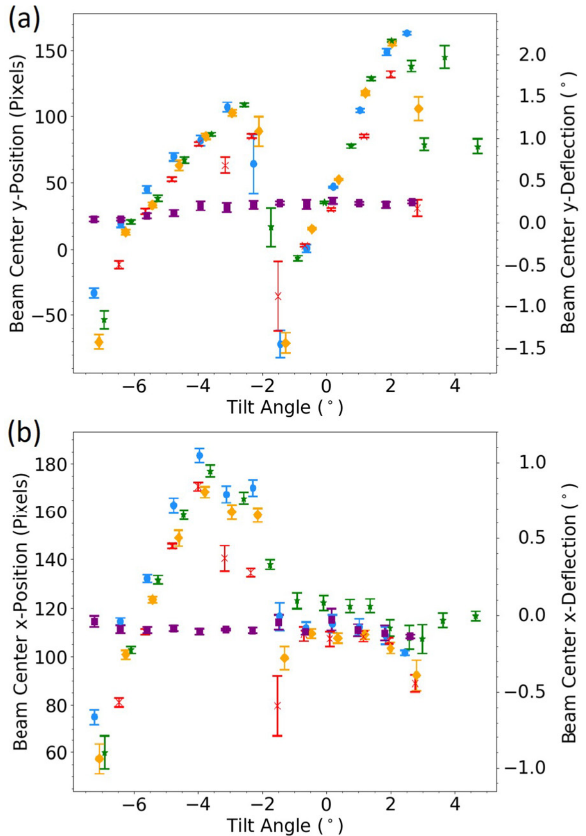


FIG. 6. (Color online) Transmitted beam peak position in pixels (left axis) and angle (right axis), as a function of stage tilt angle with respect to the Si nanomembrane normal (001) (50 nm thick membrane, 0.35 pA current) (a) $y$ and (b) $x$-directions with respect to the center of the incident beam. Symbols and colors are the same as for Fig. 5.

transmission signals occurred from channeling as indicated by the tilt angle of the two minima in the deflected intensity of Fig. 5. The angular shift in the transmitted beam position is correlated with the angular tilt away from the positions of minima. In the $y$-direction, the shifts are symmetrical with respect to the tilt angle (about the x-axis), while in the $x$-direction, they occurred only for one angular polarity.

## IV. DISCUSSION

The data are consistent with (110) and (010) planar channeling and beam steering through a Si (001) nanomembrane. The angular spacing between the two minima observed is due to a fixed mounting tilt about the $y$-axis of $5.8 \pm 0.5°$. (This tilt could not be corrected with our current set-up.) The depth of each minima increased with beam energy, as expected, since the overall transmission probability increases with energy. When incident upon an amorphous Si nanomembrane, there was no variation in transmission intensity with the incident beam angle, as expected.

The results from LAMMP simulations (30 keV) predicting the fraction of $He^+$ ion dechanneling by more than 1° have been overlaid with the measured 30 keV data (stars, green line) in Fig. 5(b). There are two examples: the first curve (upwards arrows, brown) assumed a 5.0° mounting tilt angle and no surface oxide layers while the second (triangles, black) assumed an average fixed-tilt angle 5.8° with 1 nm thick amorphous Si oxide layers on the top and bottom of the membrane. The simulations are in agreement with the detection of two planar channeling minima at positions separated by a fixed horizontal tilt angle, but the magnitudes of the dips are larger and the FWHM are smaller. The depth is a measure of the transmission efficiency of the beam and assumptions about the atomic potential and nuclear scattering cross-sections. It is clear that scattering of the channeled He through the native Si oxide layers reduces the magnitude of the dip by a significant portion toward that of the measured values. Other simulations (not shown) with only the bottom oxide layer indicated that scattering of channeled He at the bottom of the membrane explained most of the difference in the magnitudes observed.

Half the FWHM of these dips is a measure of the critical angle, $\psi_c$, for planar channeling. The data in Fig. 5 give values for $\psi_c$ of the [011] channel at 35 kV as $1.0 \pm 0.2°$ while that of the [001] channel $1.3 \pm 0.3°$. One would expect the value to be narrower for the smaller channels (100) compared to (110), but only if the axis of rotation is parallel to the planes involved. In our case, the tilt axis was parallel to the (110) planes but was 45° with respect to the (010) planes. Therefore, the FWHM for the shallower (010) minima at –5.8° would be broadened by a factor $\sqrt{2}$. The actual measured $\psi_c$ for (100) planar channeling was therefore $1.3/\sqrt{2} = 0.9°$.

The deviation in the direction of the beam as a function of the incident tilt is a clear indication that the ions were not only channeling through the Si, but partially steered by it into the channels. When the incident beam tilt was aimed down a planar channel causing a minima, the beam position was stable. Otherwise, it moved toward the channel direction by deviating in proportion to the misalignment angle. Deviations from the incident beam direction of up to 2° are evident from the maxima in the data in Fig. 6 with respect to the channeling tilt angles (0° and –5.8°). The deviation along the $y$-direction was symmetric about the positive and negative tilt directions while that of the $x$-direction was unipolar. This is understood to be due to the fixed mounting tilt about the $y$-axis such that beam steering would only occur for one polarity.

One can calculate the expected $\psi_c$ based on Lindhard theory for axial or planar channeling experiments.[1,3] The transverse energy component of an incident He ion heading toward a column of atoms is conserved, leading to a relationship between the $\psi_c$ and the average atomic potential energy, $U(r_{\min})$, at the distance of minimum approach, $r_{\min}$. It is assumed that $r_{\min}$ is given by the average thermal radius, 0.0106 nm, for Si at room temperature.[3] Electronic screening of the atomic potential can be estimated by the Thomas-Fermi equation. This depends on the average atomic spacing along the path of the ion. The wider the channel the greater the atomic density along the path traveled, and the larger the critical angle. If we had perfect axial [001] channeling, the average atomic spacing is the Si lattice constant, 0.543 nm, and the estimated $\psi_c$ is 2.8° at

35 kV. Since our nanomembrane was tilted away from the perfect [001] axial normal by –5.8° about a ⟨110⟩ axis, the atomic density along the ion path and resulting $\psi_c$ were reduced. Our experimental value of 1° means a reduction factor of 2.8, which is comparable to previously reported results from planar channeling for MeV He channeling.[3] However, another contributing effect is the influence of energy loss on the camera efficiency. Smaller count rates for ions with a 10% greater energy loss from randomly scattered directions would also mean narrower than expected channeling dips.

## V. CONCLUSIONS

In summary, we have demonstrated transmission $He^+$ ion channeling using a focussed keV He ion beam through a Si free-standing nanomembrane. We have measured the critical channeling angles for very low energy (25–35 keV) beams. Since this technique is able to measure the local transmission properties (beam spots $<1$ nm), we have potentially a method with high sensitivity to map the perfection and purity of a crystalline sample on a nanoscale. In future experiments, we will be testing this sensitivity toward the detection of local impurities and point defects, often measured in the past using MeV He ions averaging larger volumes of sample. Since 35 keV He has a wavelength in the femtometer range, beam coherence might enable visible diffraction contrast.

## ACKNOWLEDGMENTS

The work at SFU acknowledges partial support from NSERC, CFI, and 4D Labs, at U. Montreal, NSERC, Calcul Québec and Compute Canada, and at U. Wisc. DOE, Grant No. DEFG02-03ER46028s. The authors thank Norcada, Inc., Edmonton for the donation of Si membranes.

[1] G. Hlawacek, V. Veligura, R. van Gastel, and B. Poelsema, *Helium Ion Microscopy* (Springer Int., Switzerland, 2016), Chap. 9.
[2] V. Veligura, G. Hlawacek, R. van Gastel, H. J. W. Zandvliet, and B. Poelsema, Beilstein J. Nanotechnol. **3**, 501 (2012).
[3] L. C. Feldman, J. W. Mayer, and S. T. Picraux, *Materials Analysis by Ion Channeling: Submicron Crystallography* (Academic, New York, 1982).
[4] A. Vantomme, Nucl. Instrum. Methods Phys. Res., B **371**, 12 (2016).
[5] T. J. Woehl, R. M. White, and R. R. Keller, Microsc. Microanal. **22**, 544 (2016).
[6] K. L. Kavanagh, C. Herrmann, and J. A. Notte, J. Vac. Sci. Technol., B **35**, 06G902 (2017).
[7] Noranda Inc., Edmonton, AB.
[8] Z.-H. He *et al.*, Sci. Rep. **6**, 36224 (2016).
[9] X. Zhu, J. Lu, and H. Pan, Adv. Mater. Interface **4**, 1700529 (2017).
[10] G. Gopalakrishnan, D. A. Czaplewski, K. M. McElhinny, M. V. Holt, J. C. Silva-Martinez, and P. G. Evans, Appl. Phys. Lett. **102**, 033113 (2013).
[11] "LAMMPS documentation," http://lammps.sandia.gov/doc/Manual.html.
[12] R. Devanathan, T. D. de la Rubia, and W. J. Weber, J. Nucl. Mater. **253**, 47 (1998).
[13] R. Livengood, S. Tan, Y. Greenzweig, J. Notte, and S. McVey, J. Vac. Sci. Technol., B **27**, 3244 (2009).
[14] "Stopping and range of ions in matter," version SRIM-2013.00, www.SRIM.org.
[15] H. O. Funsten, S. M. Ritzau, R. W. Harper, and R. Korde, Appl. Phys. Lett. **84**, 3552 (2004).